

# X-ray Flux Related Timing and Spectral Features of 2S 1417-62

İnam, S. Çağdaş<sup>1</sup>; Baykal, Altan<sup>1</sup>; Scott, D. Matthew<sup>2</sup>; Finger, Mark<sup>2</sup>; Swank, Jean<sup>3</sup>

<sup>1</sup> Department of Physics, Middle East Technical University, İnönü Bulvarı, Balgat, Ankara 06531 Turkey

<sup>2</sup> National Space Science and Technology Center, 320 Sparkman Dr., Huntsville AL 35805 USA

<sup>3</sup> NASA Goddard Space Flight Center, Greenbelt, MD 20771 USA

9 October 2003

## Abstract

RXTE observations of the X-ray transient pulsar 2S 1417-62 between 1999 November and 2000 August with a total exposure of  $\sim 394$  ksec were analyzed. Observations include a main outburst followed by a series of mini outbursts. Changes in pulse morphology and pulse fraction were found to be related to the changes in X-ray flux. Particularly low X-ray flux regions were found to have significantly lower pulse fractions with different pulse morphologies. The 3-60 keV PCA-HEXTE main outburst spectrum was modeled with an absorbed power law model with high energy cut-off and a Gaussian Iron line complex feature. Using the same spectral model, individual 3-20 keV PCA spectra were found to be softer and less absorbed in low X-ray flux regions between outbursts. Spectral studies showed that hydrogen column density was correlated, and the power law index was anti-correlated with the 3-20 keV X-ray flux. X-ray flux related spectral and timing features in 2S 1417-62 except for low X-ray flux regions were interpreted as a sign of disc accretion with a similar accretion geometry with a varying mass accretion rate ( $\dot{M}$ ), whereas spectral and timing features of the low X-ray flux regions were interpreted as a sign of possible temporary accretion geometry change prior to the next periastron where  $\dot{M}$  increases again to restore the original accretion geometry.

**Keywords:** accretion, accretion discs - stars:neutron - X-rays:binaries - X-rays:individual: 2S 1417-62

## 1 Introduction

The X-ray source 2S 1417-62 was detected by SAS-3 in 1978 (Apparao et al. 1980). Analysis of the SAS 3 observations showed evidence of  $\sim 57$  mHz pulsations (Kelley et al. 1981). Einstein and optical observations identified a Be star companion at a distance of 1.4-11.1 kpc (Grindlay et al. 1984). From the timing analysis of BATSE observations between August 26, 1994 and July 7, 1995, orbital parameters were determined and a correlation was found between spin-up rate and pulsed flux (Finger, Wilson & Chakrabarty 1996). Orbital period and eccentricity of the source were found to be 42.12 days and 0.446 respectively.

A "Be star" is an early type non-supergiant star which has a circumstellar disc emanating from its rotational equator which is thought to be formed possibly by fast spin rotation, non-radial pulsations or magnetic loops (Slettebak 1988). Most of the Be/X-ray binary pulsar systems like 2S 1417-62 show recurrent X-ray outbursts that are thought to be mainly due to the fact that the neutron star is accreting material from the Be star's circumstellar disc (Negueruela 1998).

Table 1: Observation List for 2S 1417-62

Time of Observation day/month/year	Exposure ksec	XTE Obs ID
01-29/12/1999	58.7	40051
31/12/1999-19/01/2000	83.2	40070
22-30/11/1999 & 25/01-29/02/2000	125.0	40436
03/03-07/08/2000	127.1	50095

In this work, we will present and discuss our timing and spectral analysis of RXTE PCA observations of 2S 1417-62. In Section 2, we will present our timing and spectral analysis. In Section 3, we will discuss our results, and derive some conclusions.

## 2 Observations and Data Analysis

We analyzed RXTE archival observations of 2S 1417-62 between November 22,1999 and August 7, 2000 (See Table 1 for observation list). The results presented here are based on data collected with the Proportional Counter Array (PCA; Jahoda et al., 1996) and the High Energy X-ray Timing Experiment (HEXTE; Rothschild et al. 1998). The PCA instrument consists of an array of 5 proportional counters (PCU) operating in the 2-60 keV energy range, with a total effective area of approximately 7000 cm<sup>2</sup> and a field of view of  $\sim 1^\circ$  FWHM. Although the number of active PCU's varied between 1 and 5 during the observations, observations after 13 May 2000 belongs to the observational epoch for which background level for one of the PCUs (PCU0) increased due to the fact that this PCU started to operate without a propane layer. Latest combined background models (CM) were used together with the latest FTOOLS release (5.2) to estimate the appropriate background. The HEXTE instrument consists of two independent clusters of detectors, each cluster containing four NaI(Tl)/CsI(Na) phoswich scintillation counters (one of the detectors in cluster 2 is not used for spectral information) sharing a common  $\sim 1^\circ$  FWHM. The field of view of each cluster was switched on and off source to provide background measurements. The net open area of the seven detectors used for spectroscopy is 1400 cm<sup>2</sup>. Each detector covers the energy range 15-250 keV.

Analyzed observations consist of a main outburst that lasted for two orbital periods, followed by a series of mini outbursts each lasting for a single orbit. Duration of the main outburst and the mini outbursts are consistent with those covered in 1994 BATSE observations.

### 2.1 Timing Analysis

Background light curves were generated using the background estimator models based on the rate of very large events, spacecraft activation and cosmic X-ray emission with the standard PCA analysis tools and were subtracted from the source light curve obtained from the event data. The background subtracted light curves were corrected to the barycenter of the solar system.

Pulse frequencies for 2S 1417-62 were found by folding the time series on statistically independent trial periods (Leahy et al. 1983). Master pulses were constructed from these observations by folding the data on the period giving the maximum  $\chi^2$ . The master pulses were arranged in 20 phase bins, represented by their Fourier harmonics (Deeter & Boynton 1985), and cross-correlated with the harmonic representation of average pulse profiles from each observation. The pulse arrival times were obtained from the cross-correlation analysis. The observations of 2S 1417-62 are irregularly

Table 2: Spectral Parameters of PCA Observations of 2S 1417-62

Time (day)	$n_H$ ( $10^{22}\text{cm}^{-2}$ )	Fe Energy (keV)	Fe Sigma (keV)	Fe Norm. ( $\text{cts.cm}^{-2}.\text{s}^{-1}$ )	PL Index
50.7	$4.22 \pm 0.23$	$6.75 \pm 0.12$	$1.15 \pm 0.13$	$(1.38 \pm 0.41)10^{-3}$	$0.90 \pm 0.02$
101.9	$0.24 \pm 0.24$	$6.48 \pm 0.25$	$0.22 \pm 0.20$	$(4.98 \pm 2.50)10^{-5}$	$2.00 \pm 0.30$
126.7	$4.53 \pm 0.61$	$6.87 \pm 0.10$	$0.96 \pm 0.28$	$(3.18 \pm 1.50)10^{-4}$	$1.27 \pm 0.05$

Time (day)	PL Norm ( $\text{cts.keV}^{-1}.\text{cm}^{-2}.\text{s}^{-1}$ )	$E_{\text{cut}}$ (keV)	$E_{\text{fold}}$ (keV)	Reduced $\chi^2$ (30 d.o.f)	3-20 keV Flux (absorbed) ( $\text{ergs.cm}^{-2}.\text{s}^{-1}$ )	3-20 keV Flux (unabsorbed) ( $\text{ergs.cm}^{-2}.\text{s}^{-1}$ )
50.7	$(3.31 \pm 0.15)10^{-2}$	$11.02 \pm 0.13$	$22.71 \pm 0.63$	1.56	$9.79 \times 10^{-10}$	$1.05 \times 10^{-9}$
101.9	$(3.72 \pm 1.12)10^{-3}$	$18.03 \pm 5.00$	$30.40 \pm 6.00$	0.68	$1.17 \times 10^{-11}$	$1.17 \times 10^{-11}$
126.7	$(1.57 \pm 0.18)10^{-2}$	$10.97 \pm 0.72$	$22.27 \pm 1.95$	1.05	$1.98 \times 10^{-10}$	$2.12 \times 10^{-10}$

spaced, with many gaps of a week or more. In these gaps, pulse frequency derivatives can cause cycle count ambiguity. Therefore, we obtained the pulse frequencies using the pulse arrival times from short segments of the data spans which are typically a couple of days. Then the resulting pulse frequencies were orbitally corrected using the binary orbit parameters found from BATSE observations. In fitting of pulse frequencies for the orbit model, we left the orbital epoch as free parameter and used the the orbital parameters given by Finger et al. (1996). We found the new epoch to be JD 2551612.67  $\pm$  0.05 and the new orbital period to be 42.19  $\pm$  0.01 days, while other orbital parameters were left unchanged. Evolution of PCA count rate, pulse frequency prior to orbital correction, and orbitally corrected pulse frequency were plotted in Figure 1.

Individual pulse profiles were used to calculate pulse fractions. The relation between pulse fraction and 3-20 keV unabsorbed X-ray flux was plotted in the left panel of Figure 2. 8 pulse profiles corresponding to different flux levels were plotted in Figure 3. Spin-up rates were found by linear fitting of the  $\sim$  20 day long segments of frequency time series. In these time intervals, 3-20 keV unabsorbed X-ray flux and pulse fraction values were recalculated by averaging corresponding unabsorbed X-ray flux and pulse fraction values. Relations among frequency derivative, recalculated pulse fraction and recalculated 3-20 keV unabsorbed X-ray flux were plotted in the middle and right panels of Figure 2.

## 2.2 Spectral Analysis

Spectrum, background and response matrix files were created using *FTOOLS* 5.2 data analysis software. Background spectra were generated using the background estimator models based on the rate of very large events, spacecraft activation and cosmic X-ray emission.

Spectral analysis and error estimation of the spectral parameters were performed using *XSPEC* version 11.1. Overall PCA (3-35 keV) and HEXTE (25-60 keV) spectra were constructed for the main outburst covered by the dataset 40070 (Figure 4). Individual PCA spectra were constructed for the same time intervals that were used for calculating arrival times. Energy channels corresponding to 3-20 keV energy range were used to fit the individual PCA spectra. Energies lower than 3 keV were ignored due to uncertainties in background modelling while energies higher than 20 keV were ignored as a result of poor counting statistics. No systematic error was added to the errors.

A power law model with low energy absorption (Morrison & McCammon, 1983), multiplied by an exponential high energy cut-off function (White et al. 1983) was used to model both the overall 3-55 keV (PCA-HEXTE) spectrum and the individual 3-20 keV band (PCA) spectra. Additional Iron emission line complex modeled as a Gaussian at  $\sim$  6.4 – 6.8 keV was required as the part of the spectral model. Evolution of spectral parameters of 3-20 keV PCA spectrum was plotted

Table 3: Spectral Parameters of PCA-HEXTE Observations of the main outburst of 2S 1417-62

Parameter	Value
Hydrogen Column Density ( $10^{22} \text{cm}^{-2}$ )	$3.99 \pm 0.14$
Gaussian Line Energy (keV)	$6.82 \pm 0.16$
Gaussian Line Sigma (keV)	$1.08 \pm 0.15$
Gaussian Normalization ( $\text{cts.cm}^{-2}.\text{s}^{-1}$ )	$(1.20 \pm 0.15) \times 10^{-3}$
Power Law Photon Index	$0.90 \pm 0.02$
Cut-off Energy (keV)	$11.1 \pm 0.6$
E-folding Energy (keV)	$21.6 \pm 1.3$
Power Law Normalizations ( $\text{cts.keV}^{-1}.\text{cm}^{-2}.\text{s}^{-1}$ )	$(2.77 \pm 0.23) \times 10^{-2}$
Calculated X-ray Fluxes (3-60 keV in $\text{ergs.cm}^{-2}.\text{s}^{-1}$ )	
— Absorbed	$1.59 \times 10^{-9}$
— Unabsorbed	$1.65 \times 10^{-9}$
Reduced $\chi^2$	1.01 (119 d.o.f)

in Figure 5. Spectral parameters corresponding to the overall PCA-HEXTE spectra and these 3 regions were listed in Table 2 and 3 respectively. Using individual 3-20 keV spectra, the hydrogen column density was found to be correlated with the 3-20 keV X-ray flux, while the power-law index was found to be anti-correlated with the 3-20 keV X-ray flux (see Figure 6).

Using XSPEC software and assuming a distance of 11 kpc, 3-20 keV band luminosities were found to be  $\simeq 1.4 \times 10^{34}$  ergs/s for the low X-ray flux regions between outbursts,  $\simeq 1.3 \times 10^{36}$  ergs/s for the peak of the main outburst, and  $\simeq 2.3 \times 10^{35}$  ergs/s for the peak of the first mini outburst followed by the main outburst.

### 3 Discussion and Conclusion

In a Be/neutron star binary system, occasional X-ray outbursts may be observed, implying the neutron star is accreting material, presumably from the Be star’s circumstellar disc if the circumstellar disc undergoes a sufficiently large increase in its radial extent and density to intersect the neutron stars orbital path. The neutron star may stop accreting and ceases to be apparent as a bright X-ray source after the Be circumstellar disc has contracted.

The pattern of X-ray outbursts is affected by the size, eccentricity and orientation of the neutron star’s orbit with respect to the Be star. The orbit could be coplanar with the Be circumstellar disc or offset such that the neutron star may pass through the circumstellar disc. In the latter case, neutron star may either pass through the disc twice per orbit or pass only once per orbit as in the case for 2S 1417-62.

There are basically two accretion modes possible for the neutron star in a Be/Neutron star binary system. The first possible mode is direct accretion of the Be circumstellar disc material by the neutron star during the circumstellar disc passage in a manner similar to a wind-fed pulsar experiencing Bondi-Hoyle type accretion. For this mode, there will be less efficient angular momentum transfer compared to a standard disc accretion. This mode accretion may be considered to be the cases for the X-ray spikes during the periastron and for the mini outbursts of 2S 1845-024 (Finger et al. 1999).

The second mode that actually seems to be the case for 2S 1417-62 is accretion after the bound material has collapsed into a standard but temporary accretion disc. An accretion disc can transfer angular momentum either at the vicinity of the magnetospheric radius where the disc began to be disrupted and the material is channeled from the inner edge of the disc to the magnetic poles (via ”material torque”), or from the overall interaction of the accretion disc and magnetic field lines of

the neutron star (via "magnetic torque"). Material torque from a prograde accretion disc, being proportional to mass accretion rate, always acts to spin-up the neutron star, while the contribution of magnetic torque from the magnetic field lines threading the disc outside the corotation radius  $r_{co}$  is negative. Therefore, resultant torque can either be a spin-up (positive) or a spin-down (negative) torque.

Assuming observed X-ray luminosity is proportional to the bolometric luminosity (or mass accretion rate), spin-up rate and X-ray flux correlation can be explained by accretion from accretion disks when the net torque is positive and of the order of the material torque (Ghosh & Lamb 1979; Ghosh 1993). Correlation between spin-up rate and X-ray flux in different X-ray energy bands has been observed in outbursts of other transient X-ray pulsar systems: EXO 2030+375 (Wilson et al. 2002; Parmar, White & Stella 1989), A 0535+26 (Bildsten et al. 1997; Finger, Wilson & Harmon 1996), 2S 1845-024 (Finger et al. 1999), GRO J1744-28 (Bildsten et al. 1997), GRO J1750-27 (Scott et al. 1997), XTE J1543-568 (In't Zand, Corbet & Marshall 2001), and SAX J2103.5+4545 (Baykal, Stark & Swank 2002). Correlation between 20-50 keV X-ray flux and spin-up rate was previously found for 2S 1417-62 using BATSE observations (Finger, Wilson & Chakrabarty 1996). Our analysis of RXTE datasets of 2S 1417-62 has also showed the evidence of this correlation for both the main outburst and the following mini outbursts in 3-20 keV band (see the middle panel of Figure 2).

When the neutron star in a Be/neutron star binary system leaves the dense equatorial disc of the companion, the accretion disc can no longer be fed by the surrounding material. In this case, accretion disc may disappear and the neutron star may either continue to accrete from the non-equatorial wind of the companion or may enter the propeller phase (Illarionov & Sunyaev 1975). In case accretion is the result of the companion's non-equatorial wind, it is possible to see erratic spin-up and spin-down episodes (just like wind accreting systems, see Bildsten et al. 1997; Inam & Baykal 2000) which is not the case in 2S 1417-62 even for the lowest flux parts of our datasets. In case wind of the companion does not cause accretion, propeller phase may set in. In the propeller phase, we may expect spin pulsations to cease accompanied by a decrease in flux (Cui 1997), although it may also be the case that the pulsations do not cease completely even in the propeller phase (Neguerela et al. 2000).

Although we did not observe any erratic spin-up and spin-down episodes in the archival data, we found that both pulse fraction and shape of pulse profiles depend on the X-ray flux (Figures 2 and 3). From Figure 3, we found that the morphology of pulse profiles for the peaks of the main outburst and the mini outbursts as well as the increasing flux regions just after the periastron and declining flux regions before the next periastron passages are similar, with only a slight difference in the pulse fractions. However, both the pulse fraction and the morphology of the pulse profiles of the low flux parts of the data is considerably different from the data elsewhere. Similarity of the pulse profiles of the main outburst and the mini outbursts may indicate that we basically have the same accretion geometry with slightly different mass accretion rate. Together with the fact that the spin up rate is correlated with the flux, we may argue that we have disc accretion for all stages of the main outburst and mini outbursts with a varying mass accretion rate but basically with the same accretion geometry. Decreasing pulse fraction with changing pulse morphology for the low flux parts may indicate changes in accretion geometry and even be an indicator of a transition from disc to wind accretion, or an ongoing transition from accretor phase to propeller phase. SAX J2103.5+4545 is a counter-example for which no significant changes in pulse fraction and pulse profiles are seen with changing flux (Baykal, Stark & Swank 2002). Therefore, accretion geometry and polar cap size of SAX J2103.5+4545 should not be related considerably to the mass accretion rate while 2S 1417-62 may have such accretion geometry changes accompanied by the decrease in X-ray flux. Correlation between spin-up rate and pulse fraction is also another evidence of such a transition (see right panel of Figure 2).

Decline of the X-ray flux may be an indication of an ongoing transition from accretor to propeller stage. When the propeller stage sets in, the great majority of accreting matter cannot reach the

neutron star and factor of decrease in the bolometric luminosity becomes

$$\Delta = 170M_{1.4}^{1/3}R_6^{-1}P_0^{2/3}$$

where  $M_{1.4}$  is the mass of the neutron star in units of  $1.4M_\odot$ ,  $R_6$  is the radius of the neutron star in units of  $10^6$  cm and  $P_0$  is the spin period of the neutron star in units of second (Corbet 1996; Campana & Stella 2000; Campana et al. 2002). The factor  $\Delta$  becomes  $\sim 10^3$  for a neutron star with mass  $\sim 1.4M_\odot$ , radius  $\sim 10^6$  cm and spin period of  $\sim 17.5$  s. We do not observe such sharp X-ray flux declines in RXTE-PCA observations of 2S 1417-62, moreover a factor of  $\sim 10^3$  decrease in X-ray flux of 2S 1417-62 should be considerably less than the background level. As a comparison, 3-20 keV X-ray flux of 2S 1417-62 is lower in the low X-ray flux regions between outbursts by a factor of  $\sim 15$  with respect to peak of mini outbursts and  $\sim 90$  with respect to the peak of the main outburst. These factors seem to be considerably smaller than the expected factors for accretor to propeller transition. It is more likely that we just observe an accretion geometry change due to decreasing  $\dot{M}$ , maybe an ongoing transition to propeller, but not the propeller stage itself.

Since 2S 1417-62 is not likely to make transitions to the propeller phase, the source is probably accreting even at the lowest flux level. In case of accretion, the minimum luminosities that we have should be greater than a limiting accretion luminosity ( $L_{limit}$ ) given as: (Stella et al. 1986, Illarionov, Sunyaev 1975)

$$L_{min} > L_{limit} \cong 2 \times 10^{37} R_6^{-1} M_{1.4}^{-2/3} P_0^{-7/3} \left( \frac{\mu}{10^{30} \text{Gcm}^3} \right)^2 \text{ergs.s}^{-1}$$

where  $\mu$  ( $\cong BR^3$ , B being the surface magnetic field of the neutron star) is the magnetic moment of the neutron star. Using the spectral model for the low flux part of the data and assuming a distance of 11 kpc which is within the range of possible distances given by Grindlay et al. (1984), 0.5-30 keV X-ray luminosity is found to be  $\sim 2.1 \times 10^{34}$  ergs/s. Using this luminosity, and assuming that  $R \sim 10^6$ cm,  $M \sim 1.4M_\odot$ , a lower limit to the magnetic field can be set to be  $\sim 9 \times 10^{11}$ G, which is consistent with the typical magnetic fields of accretion powered pulsars.

From Figure 1, it is evident that the location of the periastron passage is just after the start of both the main outburst and the mini outbursts. The mini outbursts last for almost an entire orbit of 2S 1417-62 and hence indicate the binding of some Be circumstellar disc material to the neutron star during disc passage with the accretion of the bound material occurring during the course of the orbit. The BATSE observations showed a very similar normal outburst pattern with the hard X-rays (above 20 keV) starting just after the periastron passage and ending before the next periastron passage. Pattern and duration of the main outburst is also consistent with the main outburst observed by BATSE, starting just after the periastron and lasting about two orbital periods. Duration of the main outburst indicate that the equatorial disc of the companion is dense enough to provide enough disc material initially to feed the disc for two orbital periods. An increase in X-ray flux during the main outburst is observed corresponding to the periastron passage as well, showing that the neutron star has entered the equatorial disc again, but, this time, without complete depletion of the accretion disc material around it.

Galactic coordinates (l=313.02 b=-1.598) of 2S 1417-62 reveals that the source is almost at the boundary of the galactic ridge region (corresponding to R1 region defined by Valinia, Marshall 1998). Spectral model for the galactic ridge emission includes an absorbed power law model with power law index  $\sim 1.8$  and Raymond Smith component at  $\sim 3$  keV. If the flux of the galactic ridge were comparable to the X-ray flux in the low X-ray flux regions, then we would not be sure about the reality of the higher power law indices and decreasing pulse fractions, since these effects may be due to the fact that our background is contaminated by the galactic ridge emission. However, the X-ray flux in 3-20 keV is found to be only  $\sim 2.5\%$  of the typical flux for the low X-ray flux region of 2S 1417-62 by using the spectral model for R1 region of the galactic ridge. Therefore, it is not likely that our results are very much affected by the galactic ridge emission.

The spectrum of 2S 1417-62 is found to be consistent with a typical accretion powered pulsar spectral model consisting of an absorbed power law with power law index  $\sim 0.9 - 1.2$  and an high energy cut-off at  $\sim 9 - 12$  keV. For the low X-ray flux regions between outbursts, the power law index is found to be higher reaching values of  $\sim 2$ , while the cut-off energy increases to  $\sim 15 - 18$  keV but the uncertainty in the cut-off energy increases from  $\sim 0.5$  keV to  $\sim 5$  keV meanwhile.

Although the column density is, in general, found to be correlated with the X-ray flux (left panel of Figure 6), it is found to be considerably lower for the low X-ray flux regions between the outbursts where it decreases to  $\lesssim 1 \times 10^{22}$  cm $^{-2}$ . Lower hydrogen column densities together with lower X-ray flux at low X-ray flux regions may indicate lower matter concentration around the neutron star due to the fact that neutron star is in the orbital phase away from the equatorial Be wind so that matter around the neutron star has ceased or is about to cease. This is also related to the fact that the X-ray flux decreases, since  $\dot{M}$  of the accretion disc decreases due to the lower density of the surrounding material feeding the disc.

The iron line complex at  $\sim 6.4 - 6.8$  keV is found to exist for the overall data. This energy range shows that the iron line complex is composed not only of cold fluorescent Iron K line at  $\sim 6.4$  keV, but also of H-like and He-like Iron lines at  $\sim 6.7 - 7.0$  keV which is possibly emitted from hot and ionized gas around neutron star, e.g. accretion disc corona. We are unable to resolve this line complex into single emission lines in each RXTE observation. Although uncertainty in iron line energy is almost comparable to the changes in the iron line energy, there is still a weak trend that the peak energy of the iron line is found to be  $\sim 6.4 - 6.5$  keV at or near low X-ray flux parts of the data, while the peak energy reaches  $\sim 6.7 - 6.8$  keV near the X-ray flux maxima of the outbursts. A plausible explanation for this trend of the peak energy is that density of the ionized gas around the neutron star increases while outbursts occur. Future observations with new X-ray observatories like XMM-Newton and Chandra may be useful to resolve this iron line complex features in 2S 1417-62.

Anti-correlation of power law index with the X-ray flux is an indication of the fact that the spectrum gets softened with decreasing X-ray flux. (right panel of Figure 6). Spectral hardening is observed in the low state spectra of neutron star soft X-ray transients like Aql X-1, which may be interpreted to be a sign of propeller stage (Zhang et al. 1998) or a sign of a turned-on rotation powered pulsar (Campana et al. 1998). On the other hand, increasing power law indices (i.e softening of the spectra) with decreasing flux might be the consequence of mass accretion rate changes only (see e.g models for low luminosity X-ray sources by Meszaros et al. 1983; Harding et al. 1984). In this case, neither a transition to propeller stage nor an accretion geometry change is needed to explain the softening in the spectrum with decreasing flux. Consequently, decrease in mass accretion rate with a softening in the spectrum does not lead to any significant changes in pulse profiles and pulse fraction (e.g. Baykal, Stark & Swank 2002 for SAX J2103.5+4545). We have a similar situation in 2S 1417-62 except that in the lowest X-ray flux parts, the changes in pulse profiles and pulse fractions accompany spectral softening of 2S 1417-62. Therefore, spectral softening observed throughout main outburst and mini outbursts may be similar to the case in SAX J2103.5+4545, however spectral softening in 2S 1417-62 may be the result of not only accretion rate changes but also accretion geometry changes for the low flux parts, which occur just before the periastron for which the neutron star should have accreted almost all of the accretion disc material around it.

New X-ray observations which will monitor main high outbursts, the following mini outbursts and X-ray dips continuously so that the data will be continuously phase-connected will be very useful for further studies of 2S 1417-62. These observations will help us to understand the accretion mechanism better and test the possible transition from accretor to propeller stage. New observations may also be useful to revise and improve orbital parameters and to have a better understanding of timing and spectral evolution of 2S 1417-62.

#### Acknowledgments

S.Ç.İnam acknowledges the Integrated Doctorate Program scholarship from the Scientific and

Technical Research Council of Turkey (TÜBİTAK).

## References

- Apparao, K.M.V., Naranan, S., Kelley, R.L. et al., 1980, A&A 89,249  
Baykal, A., Stark, M., Swank, J., 2002, ApJ 569, 903  
Bildsten, L., Chakrabarty, D., Chiu, J. et al., 1997, ApJS 113,367  
Campana, S., Stella, L., Mereghetti, S., et al. 1998, ApJL 499, 65  
Campana, L., Stella, L., 2000, ApJ 541, 849  
Campana, S., Stella, L., Israel, G.L., et.al. 2002, ApJ 580, 389  
Corbet, R.H.D., 1996, ApJL, 457, 31  
Cui, W., 1997, ApJL, 482, 163  
Deeter, J.E., Boynton, P.E., 1985, in Proc. Inuyama Workshop on Timing Studies of X-Ray Sources, ed. S. Hayakawa & F. Nagase (Nagoya: Nagoya Univ.), 29  
Deeter, J., Crosa, L., Gerend, D. et al. 1976, ApJ, 206, 861  
Finger, M.H., Wilson, R.B., Chakrabarty, D., 1996, A&ASS 120, 209  
Finger, M.H., Wilson, R.B., Harmon, B.A., 1996, ApJ 459, 288  
Finger, M.H., Bildsten, L., Chakrabarty, D. et al. 1999, ApJ 517,449  
Ghosh, P., Lamb, F.K., 1979, ApJ 234, 296  
Ghosh, P. 1993, The Evolution of X-ray binaries, eds. S.S.Holt & C.S.Day, p439  
Grindlay, J.E., Petro, L.D., McClintock, J.E., 1984, ApJ 276, 621  
Harding, A.K., Meszaros, P., Kirk, J.G. et al. 1984, ApJ 278, 369  
Illarionov, A.F., Sunyaev, R.A., 1975, A&A. 39, 185  
İnam, S.C., Baykal, A., 2000, A&A 353, 617  
in't Zand, J.J.M., Corbet, R.H.D., Marshall, F.E. 2001, ApJL 553, 165  
Jahoda, K., Swank, J.H., Giles, A.B. et al. 1996, Proc.SPIE, 2808, 59  
Kelley, R.L., Apparao, K.M.V, Doxsey, R.E. et al., 1981, ApJ 243, 251  
Leahy, D.A., Darbo, W., Elsner, R.F. et al. 1983, ApJ 266, 160  
Meszaros, P., Harding, A.K., Kirk, J.G. et al. 1983 ApJL 266, 33  
Morrison, R., McCammon, D., 1983, ApJ 270,119  
Negueruela, I., 1998, A&A 338,505  
Negueruela, I., Reig, P., Finger, M.H. et al. 2000, A&A, 356, 1003  
Parmar, A.N., White, N.E., Stella, L., 1989, ApJ 184, 271  
Rotschild, R.E., Blanco, P.R., Gruber, D.E. et. al. 1998, ApJ, 496, 538  
Scott, D.M, Finger, M.H., Wilson, R.B. et al. 1997, ApJ, 488, 831  
Slettebak, A., 1988, PASP 100,770  
Stella, L., White, N.E., Rosner, R., 1986, ApJ 308, 669  
Valinia, A., Marshall, F.E., 1998, ApJ 505, 134  
White, N.E, Swank, J.H., Holt, S.S. 1983, ApJ 270,711  
Wilson, C.A., Finger, M.H., Coe, M.J., et al., 2002, ApJ 570, 287  
Zhang, Z.N, Yu, W., Zhang, W., 1998, ApJL 494, 71



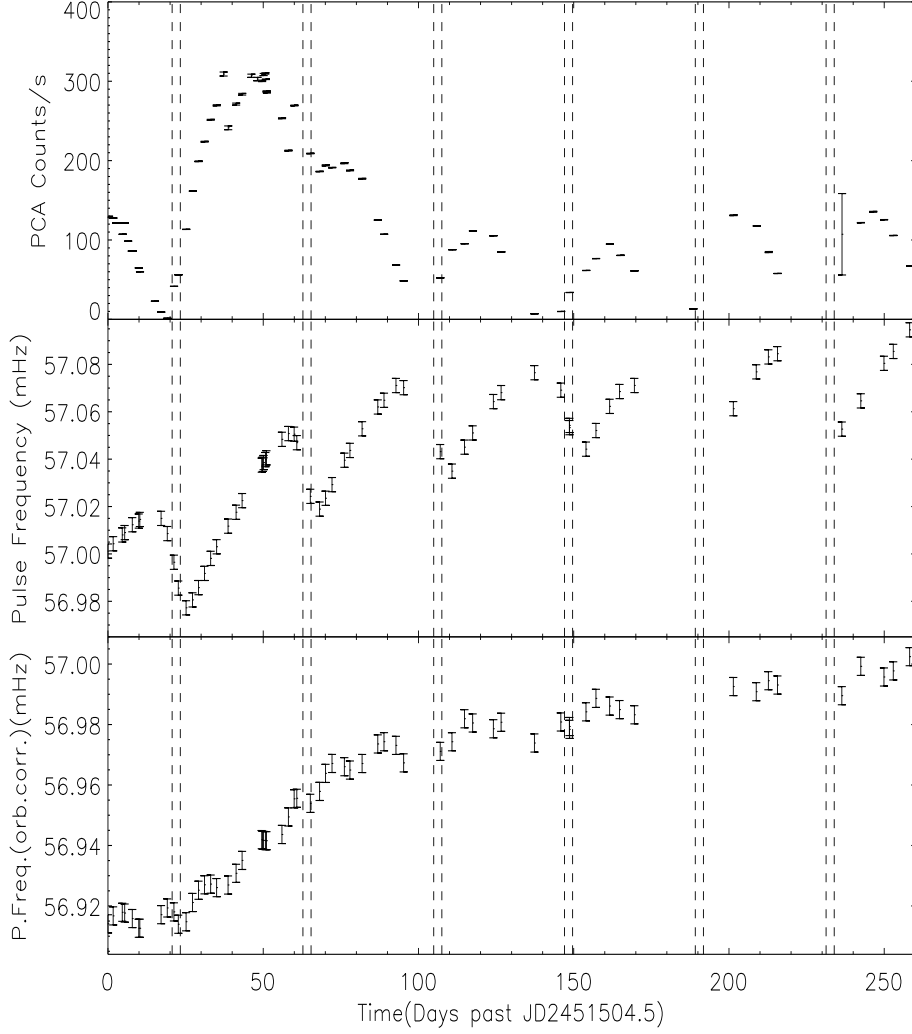


Fig. 1.— Background subtracted PCA count rate normalized to 5 PCUs in 3-20 keV band, frequency history before and after orbit subtraction are plotted against time. Initial time value corresponds to November 22, 1999, while the peak of the main outburst is about 50 days later than this date. Note that in some parts of the data, frequencies could not be estimated. These frequency values were left blank. All of the errors are in  $1\sigma$  level. Vertical dashed lines indicate the orbital phase corresponding to periastron passages.

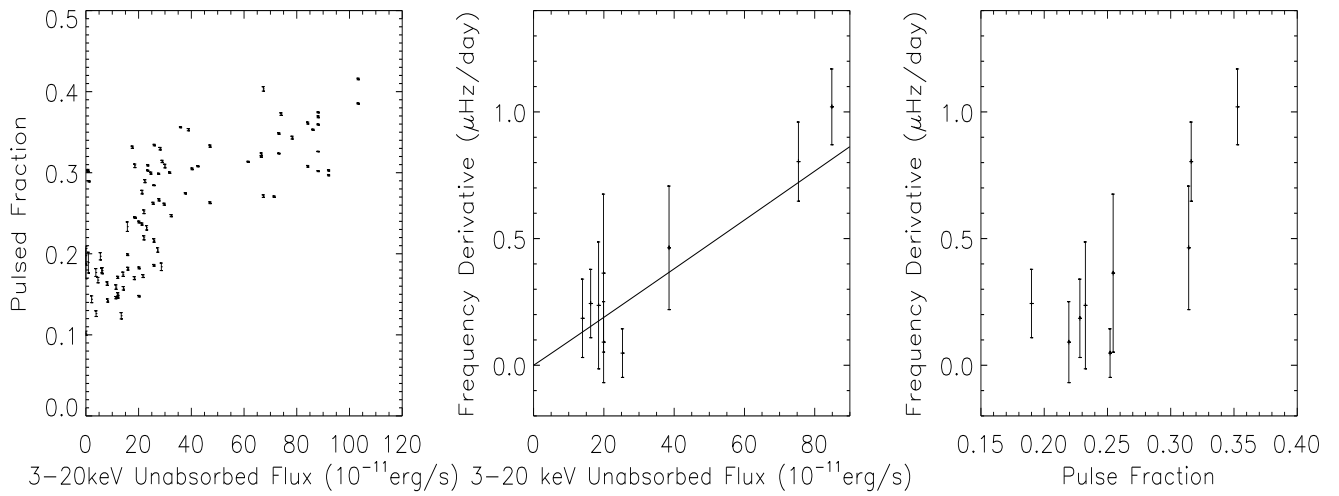


Fig. 2 – **(left)** Pulse fraction versus 3-20 keV unabsorbed X-ray flux.  $(F_{max} - F_{min})/(F_{max} + F_{min})$  definition is used to calculate pulse fractions where  $F_{max}$  and  $F_{min}$  are the highest and lowest fluxes of the phase bins. **(middle)** Pulse Frequency Derivative versus 3-20 keV unabsorbed X-ray flux. Frequency derivatives were found by linear fitting of  $\sim 20$  day intervals of frequency history. X-ray fluxes were found by averaging the corresponding X-ray flux values. Solid line indicates best power law fit with the power index 1.01. **(right)** Pulse frequency derivative versus pulse fraction. Pulse frequency derivatives from the middle panel of this figure were plotted against pulse fractions which were found by averaging corresponding pulse fraction values. Errors in all of the panels are in  $1\sigma$  level.

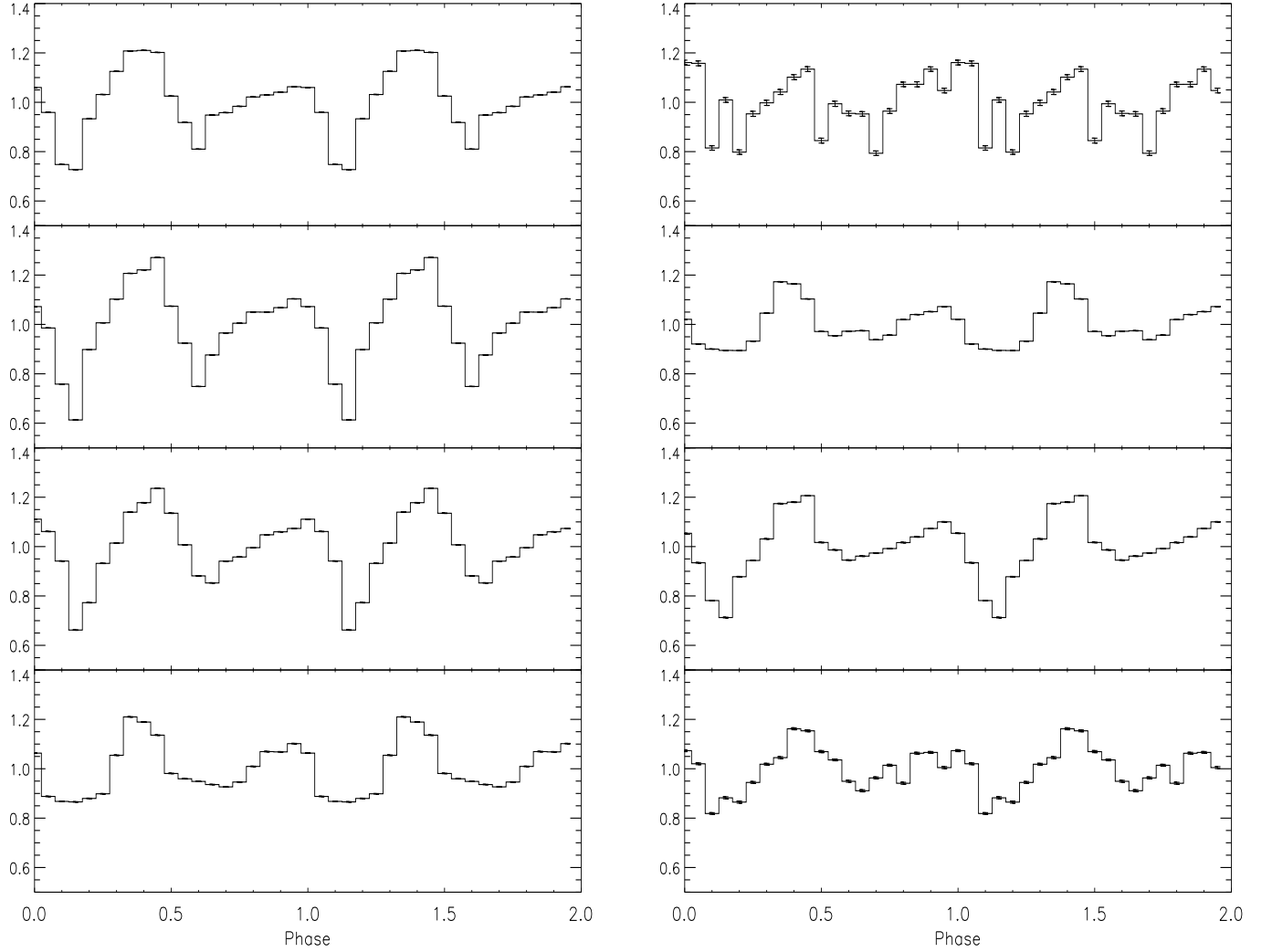


Fig. 3 – **(left)** Pulse profiles for days  $\sim 31.2$  (rise of the main outburst),  $\sim 50.6$  (peak of the main outburst),  $\sim 76.2$  (peak of the main outburst at the second orbit),  $\sim 95.3$  (decline of the main outburst), **(right)**  $\sim 101.9$  (low X-ray flux part),  $\sim 107.1$  (rise of the mini outburst),  $\sim 124.1$  (peak of the mini outburst), and  $\sim 137.4$  (decline of the mini outburst). Corresponding 3-20 keV unabsorbed fluxes in units  $10^{-11}\text{ergs.cm}^2.\text{s}^{-1}$  are 75.1, 105.1, 54.0, 11.9, 1.18, 11.9, 21.9, and 3.69 respectively. Phases of the pulse profiles were manually aligned, using the similarities in the pulse shapes and the positions of primary and secondary peaks.

PCA and HEXTE Spectra of 2S 1417–62

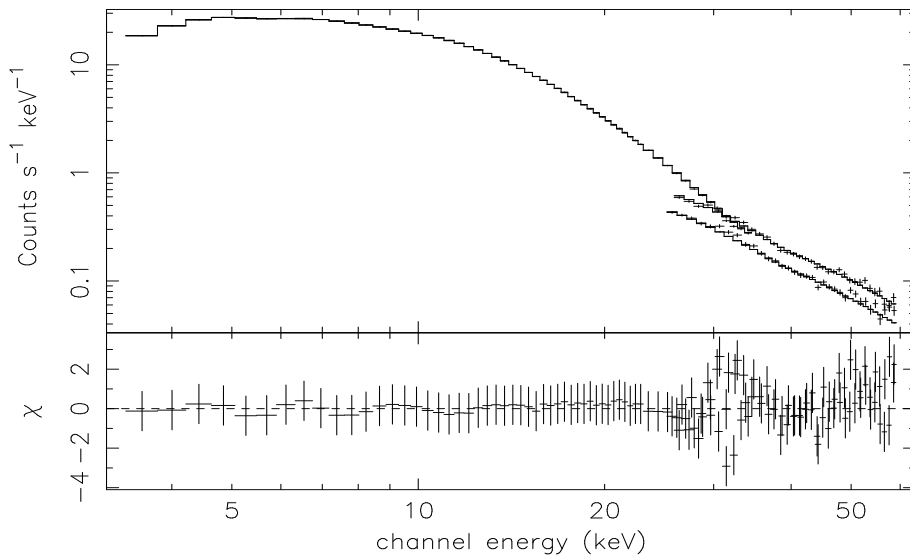


Fig. 4 – Combined PCA and HEXTE spectrum for the dataset 40070. The bottom panel shows the residuals of the fit in terms of  $\sigma$  values.

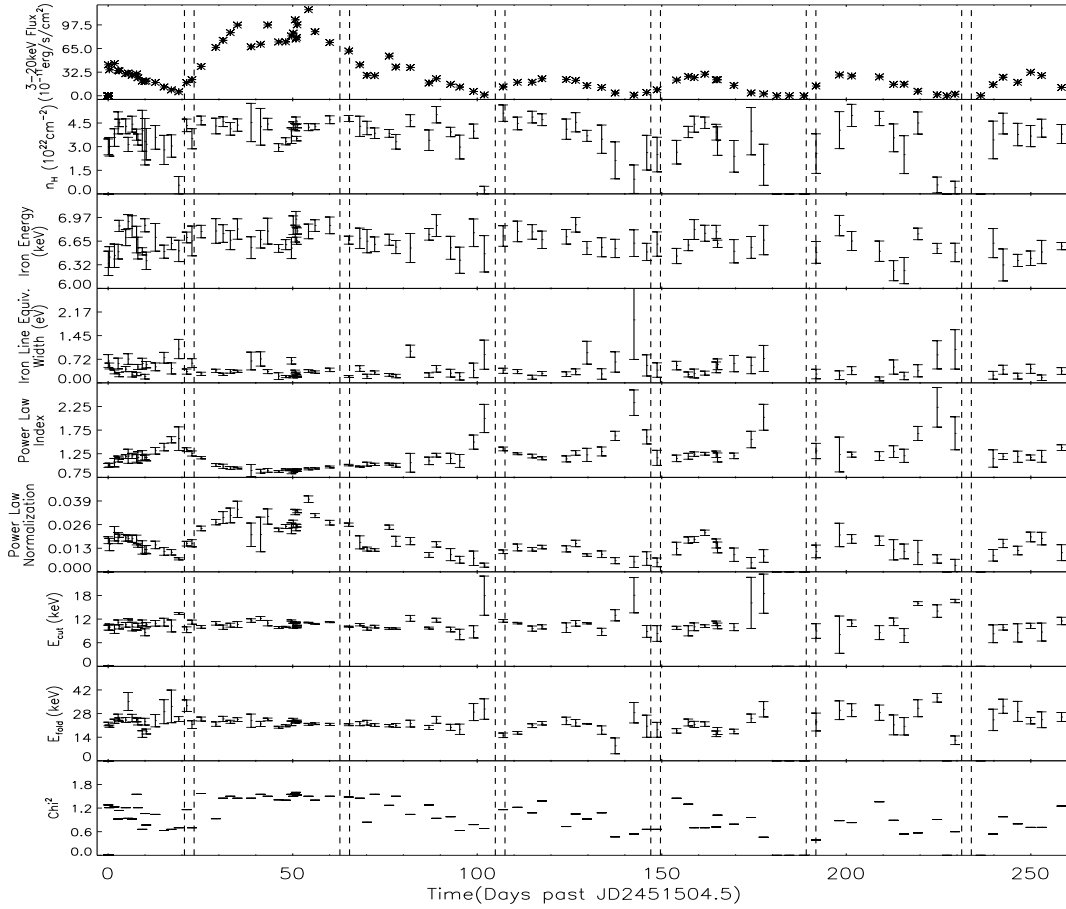


Fig. 5 – Evolution of Hydrogen column density, Iron line complex peak energy, iron line equivalent width, power law index, power law normalization, cut-off energy, folding energy, and reduced  $\chi^2$ . Vertical dashed lines indicate the orbital phase corresponding to periastron passages.

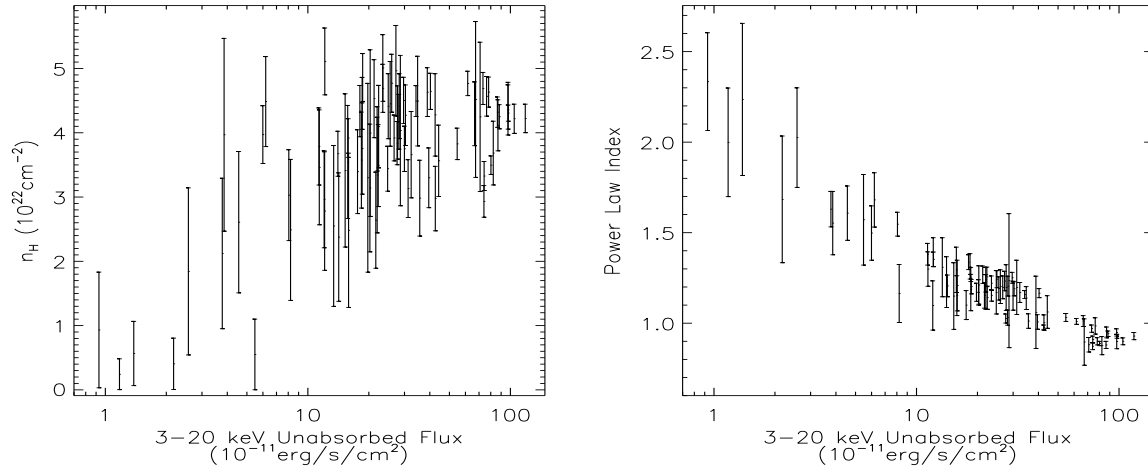


Fig. 6 – **(left)** Hydrogen column density as a function of 3-20 keV unabsorbed X-ray flux. **(right)** Power law index as a function of 3-20 keV unabsorbed X-ray flux.